

www.acsami.org Research Article

# Surface Embedded Metal Nanowire—Liquid Metal—Elastomer Hybrid Composites for Stretchable Electronics

Darpan Shukla, Hongyu Wang, Omar Awartani, Michael D. Dickey, and Yong Zhu\*



Cite This: ACS Appl. Mater. Interfaces 2024, 16, 14183–14197



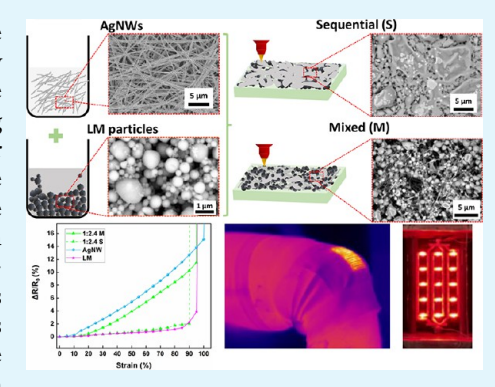
**ACCESS** I

III Metrics & More

Article Recommendations

s Supporting Information

ABSTRACT: Both liquid metal (LM) and metallic filler-based conductive composites are promising stretchable conductors. LM alloys exhibit intrinsically high deformability but present challenges for patterning on polymeric substrates due to high surface tension. On the other hand, conductive composites comprising metallic fillers undergo considerable decrease in electrical conductivity under mechanical deformation. To address the challenges, we present silver nanowire (AgNW)-LM-elastomer hybrid composite films, where AgNWs and LM are embedded below the surface of an elastomeric matrix, using two fabrication approaches, sequential and mixed. We investigate and understand the process–structure—property relationship of the AgNW-LM-elastomer hybrid composites fabricated using two approaches. Different weight ratios of AgNWs and LM particles provide tunable electrical conductivity. The hybrid composites show more stable electromechanical performance than the composites with AgNWs alone. In



particular, 1:2.4 (AgNW:LMP w/w) sequential hybrid composite shows electromechanical stability similar to that of the LM-elastomer composite, with a resistance increase of 2.04% at 90% strain. The sequential approach is found to form AgIn<sub>2</sub> intermetallic compounds which along with Ga—In bonds, imparts large deformability to the sequential hybrid composite as well as mechanical robustness against scratching, cutting, peeling, and wiping. To demonstrate the application of the hybrid composite for stretchable electronics, a laser patterned stretchable heater on textile and a stretchable circuit including a light-emitting diode are fabricated.

KEYWORDS: silver nanowire, liquid metal, stretchable electronics, hybrid composite, intermetallic alloy, sintering

## 1. INTRODUCTION

Stretchable electronics have recently received much interest. 1-6 Conductive composites that are composed of nanomaterial-based conductive fillers such as metal nanowires, metal nanoparticles, graphene, and carbon nanotubes (CNTs) dispersed in an elastomeric matrix are commonly used in stretchable electronics.<sup>7-11</sup> Incorporation of these conductive fillers in an elastomer provides mechanical deformability such as flexibility and stretchability. 12-15 However, conventional conductive composites comprise only one type of conductive fillers. Typically, these single-filler composites require high filler loading to reach percolation, which compromises stretchability of the elastomer-based composites. They also undergo a significant increase in the electrical resistance upon mechanical deformation due to degradation of the percolating network under strain, i.e., separation of the conductive fillers. 16-20 To counter these issues, conductive composites with more than one type of conductive fillers have been developed, termed as hybrid-filler (or hybrid) composites.<sup>21</sup>

Hybrid composites with multiple fillers can synergistically improve the mechanical and electrical performances of composites. <sup>22–25</sup> In particular, additional fillers such as liquid metal (LM) can bridge the gaps between the primary fillers and can thus improve the electromechanical behavior of the

composite, i.e., a more stable conductivity under strain. 26,27 For instance, conductors that maintain continuity to 1000% strain were demonstrated by combining different types of silver (Ag)-based conductive fillers and eutectic gallium-indium (EGaIn) particles in elastomer. EGaIn particles act as electrical anchors between the Ag-based conductive fillers and improved the conductivity, stretchability, and cyclic durability of the superelastic conductor. 16 Highly elastic and stretchable multilayer circuits that could withstand 600% strain were printed using Ag flakes and EGaIn as conductive fillers in a styrene-isoprene-rubber binder. The composite achieved ~5 times higher stretchability and ~27 times higher quality factor than Ag flake-based single-filler composite. Note that quality factor is defined as the ratio of mechanical strain over relative change in electrical resistance; larger quality factor means more stable electrical resistance. 28 The large improvement in performance was attributed to room-temperature sintering of

Received: January 6, 2024
Revised: February 23, 2024
Accepted: February 27, 2024
Published: March 8, 2024





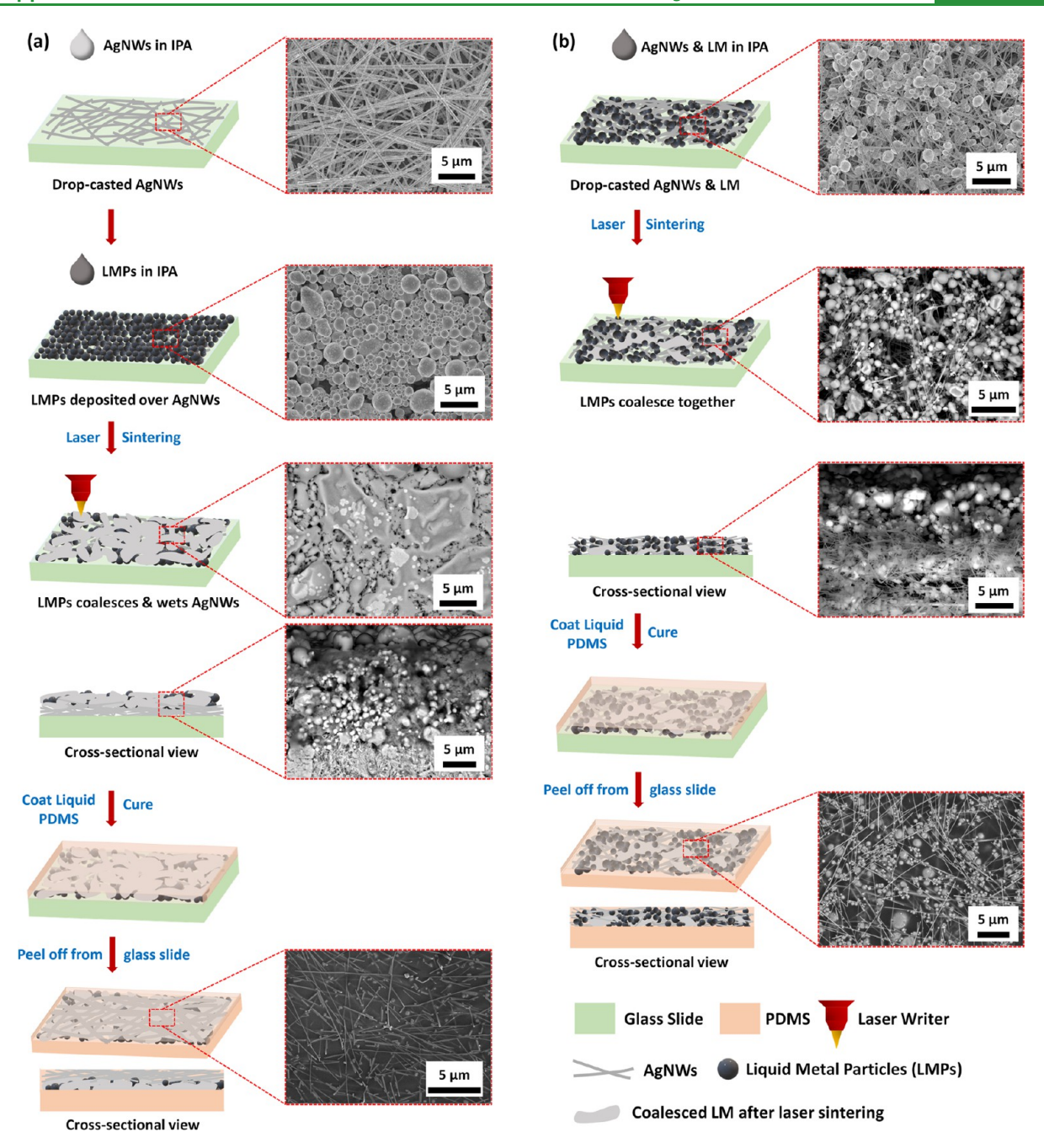


Figure 1. Schematic illustrating (a) Fabrication of AgNW-LM film and surface embedded AgNW-LM-PDMS hybrid composite from sequential approach (abbreviated as S). Top to bottom insets showing top-view SEM image of drop-casted AgNWs, top-view SEM image of unsintered AgNW-LM film, top-view SEM image of laser sintered AgNW-LM film, cross-sectional view SEM image of AgNW-LM film and top-view SEM image of surface embedded AgNW-LM-PDMS hybrid composite (Scale bar: 5 µm). (b) Fabrication of AgNW-LM film and surface embedded AgNW-LM-PDMS hybrid composite from mixed approach (abbreviated as M). Top to bottom insets showing top-view SEM image of unsintered AgNW-LM film, top-view SEM image of laser sintered AgNW-LM film, cross-sectional view SEM image of AgNW-LM film and top-view SEM image of surface embedded AgNW-LM-PDMS hybrid composite (Scale bar: 5  $\mu$ m).

the Ag flakes with EGaIn to form AgIn<sub>2</sub> microparticles, Ga-In droplets, and Ag flakes that were surrounded by Ag-In and Ga-In alloys. Similarly, conductive polymer composites consisting of CNTs/carbon nanofibers (CNFs) and LM (Galinstan) as multiphase hybrid fillers were fabricated. Under strain, the oxide shell broke exposing the LM in the core, which then bridged the gaps between CNTs/CNFs, maintaining a stable electrical connection.<sup>26</sup>

Among metal-based conductive fillers, metal nanowires with high aspect ratios such as Ag nanowires (AgNWs) have received considerable attention due to their high electrical conductivity and ability to form percolation network at relatively low threshold. 11,29-32 Therefore, hybrid composites with AgNWs and LM as fillers are becoming increasingly popular.<sup>33,34</sup> In one such work, a freestanding thin film conductor was developed by incorporating AgNWs and EGaIn particles followed by selective laser sintering and selective chemical etching of the film. High electrical conductivity of  $5.79 \times 10^5 \text{ S m}^{-1}$  and high stretchability of 1350% were achieved due to the wettability between AgNWs and EGaIn

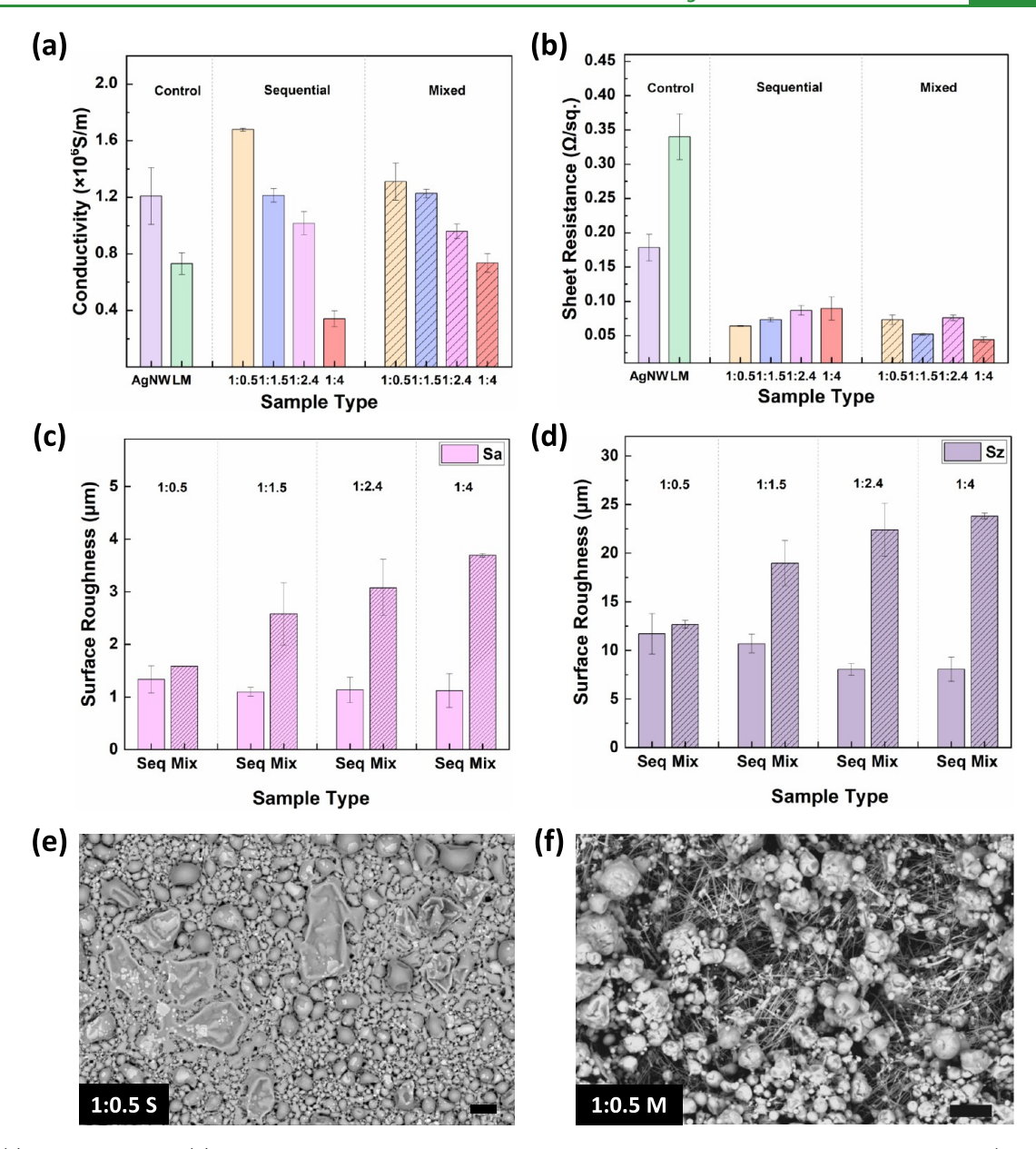


Figure 2. (a) Conductivity and (b) Sheet resistance of AgNW, LM, and AgNW-LM films with different ratios of AgNW:LMP (w/w) fabricated using sequential and mixed approach. Three samples were tested for each case. For the control, the AgNWs were thermally annealed at 150 °C and the LMPs were laser sintered. (c) Surface roughness parameter arithmetic mean height ( $S_a$ ) for AgNW-LM films from sequential and mixed approach for different weight ratios of AgNW:LMP. (d) Surface roughness parameter maximum peak-to-valley height ( $S_a$ ) for AgNW-LM films from sequential and mixed approach for different weight ratios of AgNW:LMP. Three samples were tested for each case in (c) and (d). Top-view SEM images of laser sintered 1:0.5 w/w AgNW-LM film fabricated using (e) sequential approach (abbreviated as S) and (f) mixed approach (abbreviated as M). Scale bar: 5  $\mu$ m.

after laser sintering, and high deformability of EGaIn.<sup>35</sup> In all these works, the fabrication involved mixing sonicated LM particles with AgNWs.<sup>33–36</sup> However, no sequential fabrication, i.e., depositing LM particles on top of AgNWs, has been reported, nor was there research on how different fabrication approaches impact the structure and performances of the hybrid composites.

In this work, we present two different approaches, i.e., sequential and mixed, to fabricate hybrid composites incorporating AgNWs as metal-based conductive fillers with high aspect ratio and EGaIn as LM particles (LMPs) into an elastomeric matrix, e.g., polydimethylsiloxane (PDMS) (Figure 1). The AgNWs and LMPs are embedded below the surface of

the matrix as shown in Figure 1. The hybrid composites fabricated using the two approaches were thoroughly investigated in terms of morphology, electrical conductivity, and electromechanical stability. The AgNW-LM films from both approaches produced tunable electrical conductivity and surface roughness with varying weight ratios of AgNW:LMP. Additionally, films fabricated using the sequential approach showed the formation of  $AgIn_2$  intermetallic compound which provided the composite its mechanical robustness, whereas LM provided fluid-like deformability. The AgNW-LM-elastomer hybrid composites, fabricated by either approach, showed better electromechanical stability than the AgNW-elastomer composite. Particularly, the 1:2.4 w/w sequential hybrid

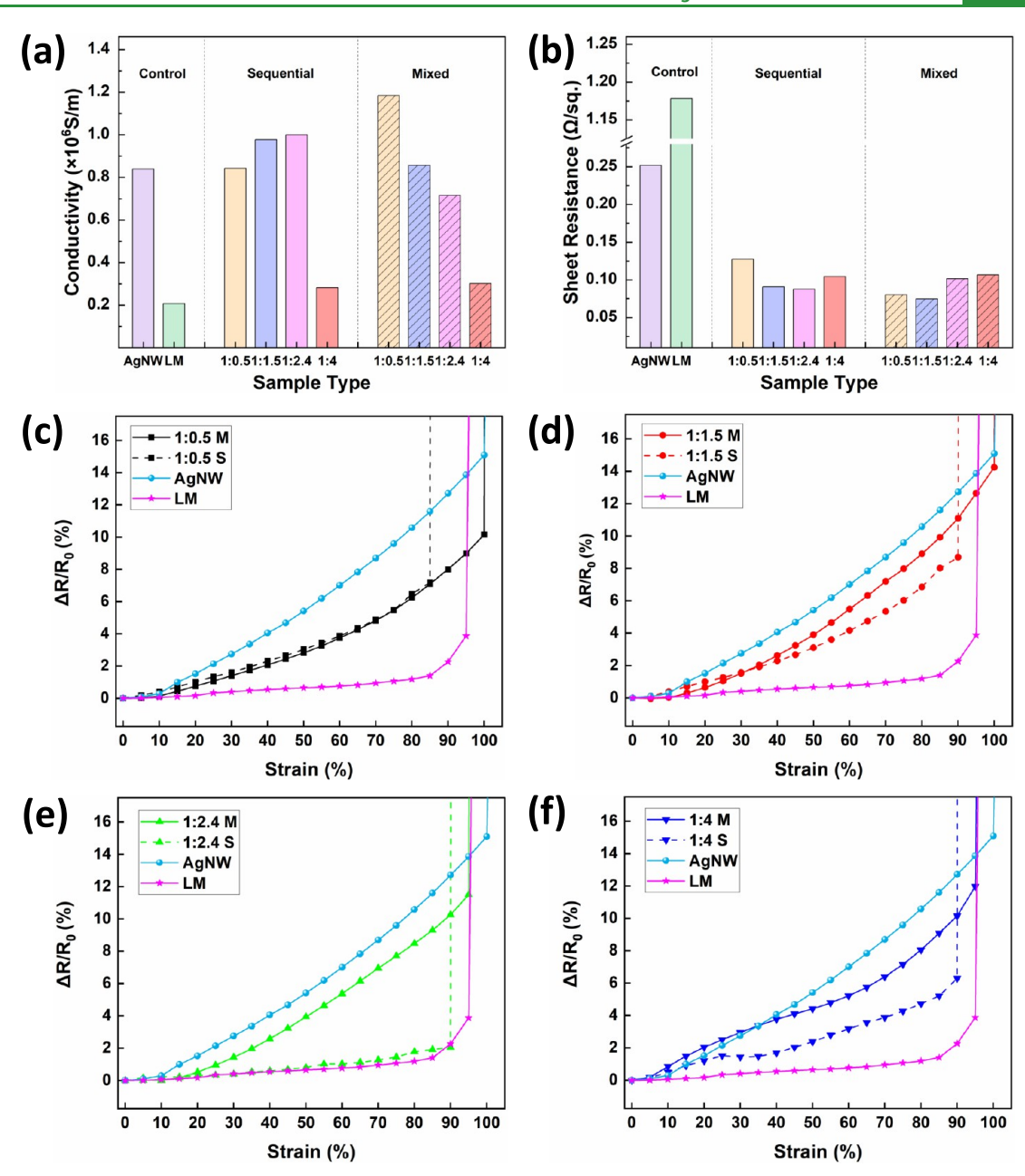


Figure 3. (a) Conductivity and (b) Sheet resistances of AgNW-PDMS composite, LM-PDMS composite, surface embedded sequential AgNW-LM-PDMS hybrid composite, and surface embedded mixed AgNW-LM-PDMS hybrid composite with different ratios of AgNW:LMP (w/w). Resistance change as a function of strain for AgNW-PDMS composite, LM-PDMS composite, surface embedded sequential AgNW-LM-PDMS hybrid composite (S), and surface embedded mixed AgNW-LM-PDMS hybrid composite (M) until failure for AgNW:LMP (w/w) (c) 1:0.5, (d) 1:1.5 (e) 1:2.4, and (f) 1:4.

composite showed the best electromechanical stability, i.e., a resistance increase of only 2.04% at 90% strain, similar to that of the LM-elastomer composite. The hybrid composite was also mechanically robust against scratching, cutting, peeling, and wiping. To demonstrate the application for stretchable electronics, a laser patterned stretchable heater on textile and a stretchable circuit including a light-emitting diode (LED) were fabricated.

#### 2. RESULTS AND DISCUSSION

The AgNW-LMP based hybrid composites were fabricated using two different approaches—sequential approach and mixed approach. For either approach, AgNW-LM film was fabricated, and then uncured elastomer was spin-coated on top

to form the hybrid composite. Here we start with the fabrication and characterization of the AgNW-LM film. First, AgNWs were synthesized using modified polyol method and suspended in isopropanol (IPA). <sup>37,38</sup> Next, LMP solution was prepared through tip sonication of bulk EGaIn in IPA, as shown in Figure S1. Various methods have been reported to remove the oxide layer to the LM with the most common ones being mechanical sintering, <sup>39</sup> laser sintering, <sup>33</sup> and chemical treatment with either a strong acid (HCl) or a base (NaOH). <sup>40</sup> In this work, we chose laser sintering using a CO<sub>2</sub> based laser for rapid, high-resolution sintering. <sup>41</sup> Additionally, the same laser was used for direct patterning of both the AgNW-LM film and the hybrid composite. In the sequential approach (Figure 1a), the AgNW solution was first drop-casted on a glass

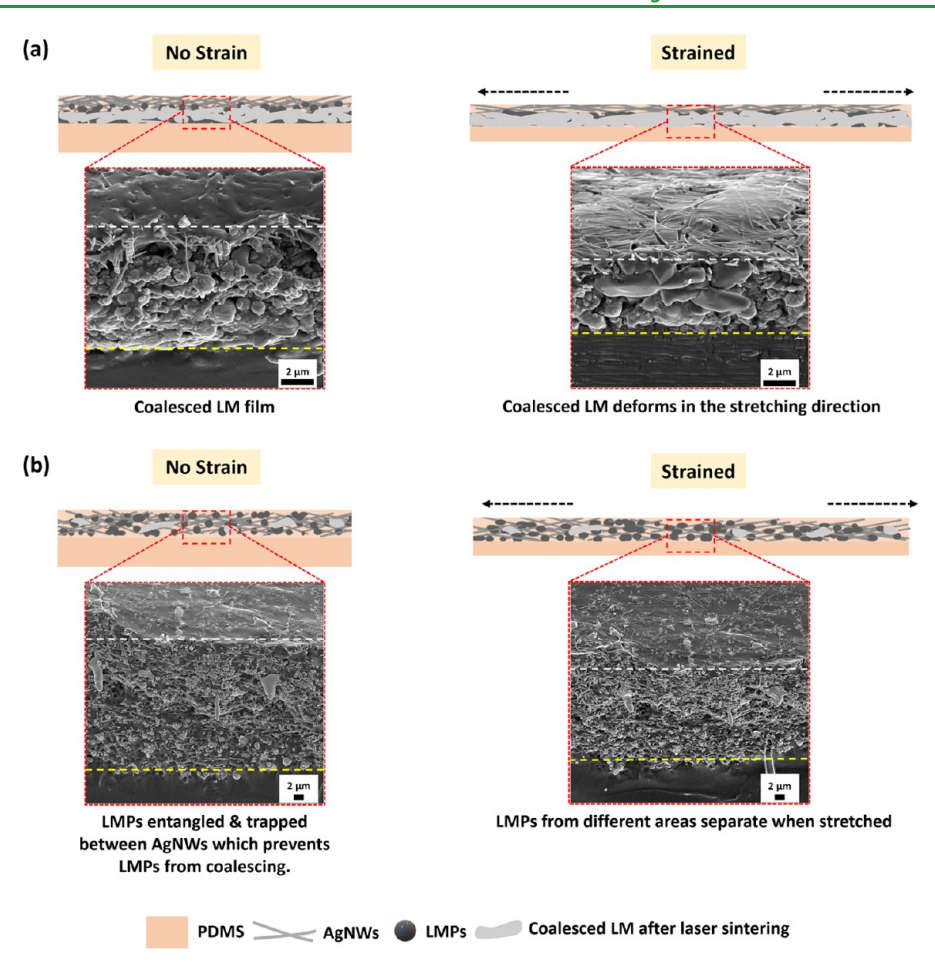


Figure 4. (a) Schematic illustrating the behavior of sequential surface embedded AgNW-LM-PDMS hybrid composite under no strain and strain. Left to right inset showing 0° and 25° titled cross-sectional view SEM images before and after strain. Scale bar: 2 µm. (b) Schematic illustrating the behavior of surface embedded mixed AgNW-LM-PDMS hybrid composite under no strain and strain. Left to right inset showing 50° titled crosssectional view SEM images before and after strain. Scale bar: 2 µm. White dashed line represents the interface between the top surface and crosssectional views. The yellow dashed line represents the interface for the cross-sectional view.

substrate and dried in a convection oven at 50 °C. Next, the LMP solution was deposited over the AgNW network and dried. The AgNW-LMP film was laser sintered to break the oxide shell of LMPs. 41,42 The exploded LMP core covers the surface of AgNWs and coalesces with the neighboring LMPs.<sup>33</sup> For fabricating the surface embedded AgNW-LM-PDMS sequential hybrid composite, uncured PDMS was spin coated on top of the AgNW-LM film. In the mixed approach (Figure 1b), the AgNW solution was mixed with the LMP solution in different weight ratios of AgNW and LMP. The mixed solution was then drop-casted on a glass substrate and dried in a convection oven at 50 °C. The AgNW-LMP film was laser sintered to wet the AgNWs by LM and also fuse with the neighboring LMPs. Similar to the sequential hybrid composite, uncured PDMS was spin-coated on top of the AgNW-LM film to fabricate surface embedded mixed hybrid composite. Table S1 shows the laser sintering conditions for the AgNW-LM films fabricated using the two approaches.

AgNW-LM films were fabricated using both sequential and mixed approaches with different weight ratios of AgNW:LMP (same weight of AgNWs). In this work, the weight ratios of AgNW:LMP were varied as 1:0.5, 1:1.5, 1:2.4, and 1:4. The weight ratio higher than 1:4 resulted in poor embedding of the conductive fillers in the elastomer, as shown in Figure S2. Figure 2a,b shows that changing the weight ratio of AgNW:LMP in the film can lead to tunable electrical conductivity. Electrical conductivity of AgNW-LM films fabricated using the sequential approach changed from (1.68  $\pm 0.01$ )  $\times 10^{6}$  to  $(3.41 \pm 0.57) \times 10^{5}$  S m<sup>-1</sup> with the AgNW:LMP (w/w) ratio varying from 1:0.5 to 1:4. Whereas, for the same weight ratio, films fabricated using the mixed approach showed electrical conductivity varying from (1.31 ±  $0.13) \times 10^6$  to  $(7.36 \pm 0.69) \times 10^5$  S m<sup>-1</sup>. Lower electrical conductivity of the sequentially fabricated 1:4 (w/w) AgNW-LM film might be related to the limited laser sintering depth. 41,43,44 The sheet resistances of the AgNW-LM films with the sequential and mixed approaches varied from (0.064  $\pm 0.001$ ) to  $(0.090 \pm 0.017) \Omega \text{ sq}^{-1}$  and from  $(0.073 \pm 0.007)$ to (0.044  $\pm$  0.004)  $\Omega$  sq<sup>-1</sup>, respectively, with the increasing LM content.

Morphologies and microstructures of the AgNW-LM films fabricated using the two approaches were examined by confocal microscopy imaging. Figure 2c illustrates that for the same AgNW:LMP weight ratio, arithmetic mean height  $(S_a)$  of the film from the mixed approach is higher than that from the sequential approach. For instance, the  $S_a$  for the 1:4 (w/w) AgNW-LM films fabricated from the sequential and mixed approach was 1.12 and 3.69  $\mu$ m, respectively. Similarly, Figure 2d shows a higher peak-to-valley height  $(S_z)$  for the films fabricated using the mixed approach.  $S_z$  for the 1:4 (w/w)

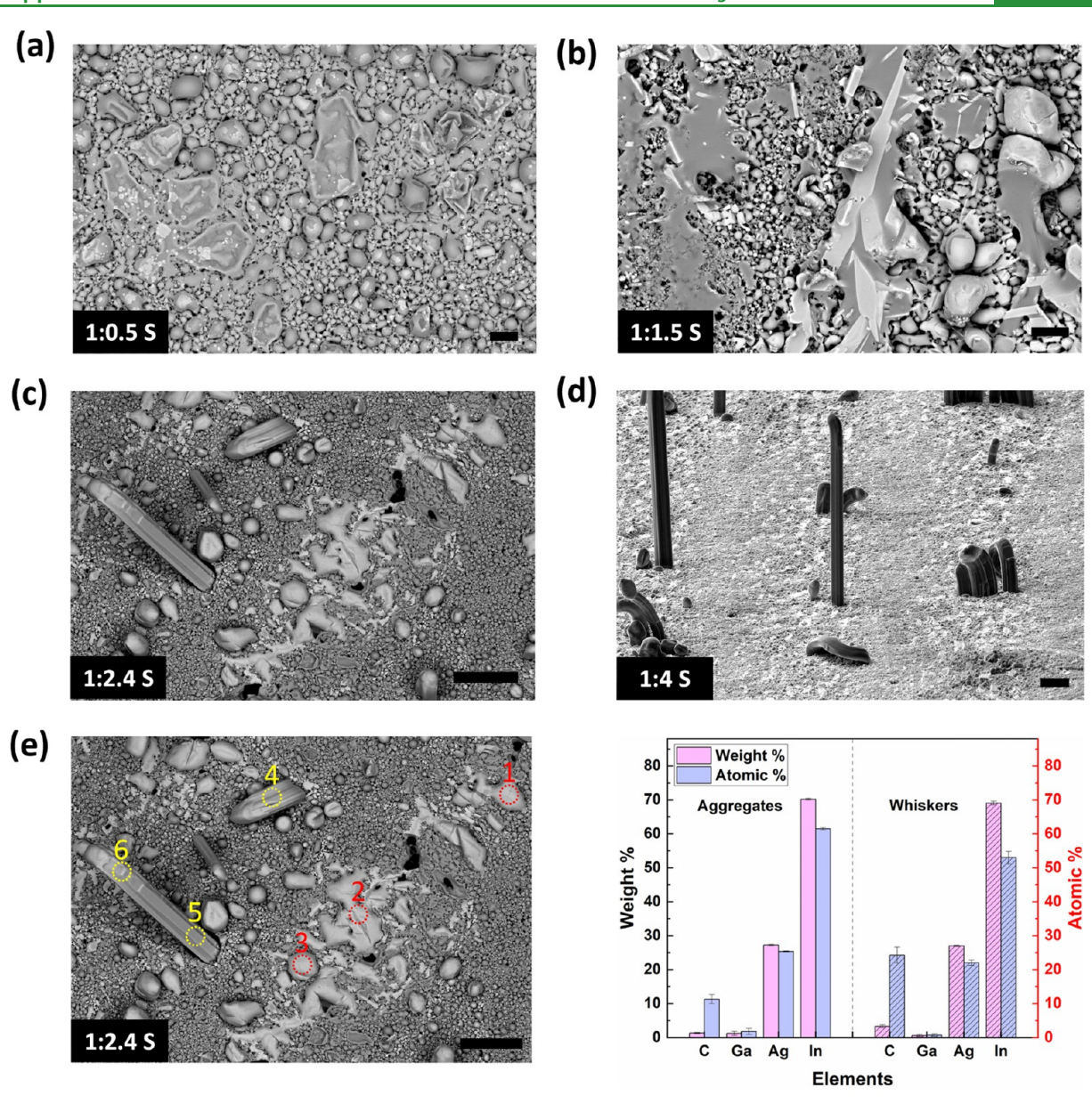


Figure 5. Top-view SEM images of sequentially fabricated AgNW-LM films (S) at different AgNW:LMP (w/w) ratios of (a) 1:0.5, (b) 1:1.5, (c) 1:2.4, and (d) 1:4. Scale bar: 5  $\mu$ m. (e) Top-view SEM image and EDS point elemental analysis for sequentially fabricated AgNW-LM film with 1:2.4 wt % AgNW:LMP. Scale bar: 25  $\mu$ m. Points 1–3 correspond to the Ag–In aggregates, while points 4–6 correspond to Ag–In whiskers.

AgNW-LM films fabricated from the sequential and mixed approach was 8.05 and 23.81  $\mu$ m, respectively. Figure S3a depicts that the surface roughness of the AgNW-LM films produced using the sequential approach decreases with the increasing LM content. This is attributed to the formation of a uniform coalesced LMP layer on top of the AgNWs, as shown in the top-view scanning electron microscopy (SEM) image of the 1:0.5 (w/w) AgNW-LM film (Figure 2e). On the contrary, the average surface roughness of the films with the mixed approach increases with the increasing LM content (Figure S3b) because of increased entanglement of AgNWs and LMPs.<sup>33</sup> Figure S4 shows increased formation of lumped debris of the entangled AgNWs and LMPs with increasing LM amount. Figure 2f illustrates the entangled AgNWs and LMPs in a top-view SEM image of the 1:0.5 (w/w) AgNW-LM film as an example. Surface roughness of the AgNW-LM film plays

a crucial role in the efficiency of laser sintering as the uneven surface affects the laser focusing.  $^{33}$ 

As shown in Figure 1, on top of the AgNW-LM film (fabricated by either approach), uncured PDMS was spin-coated; due to its low viscosity and low surface energy, PDMS can infiltrate through the porous AgNW-LM structure. After curing the PDMS, the film was peeled off the glass slide to form a surface embedded AgNW-LM-PDMS hybrid composite. Similarly, AgNW-PDMS and LM-PDMS composites were fabricated as single-filler composites for the purpose of comparison. Figure 3a displays the electrical conductivity of the surface embedded AgNW-LM-PDMS hybrid composites from both sequential and mixed approach along with the AgNW-PDMS and LM-PDMS composite. For the AgNW:LMP ratios of 1:0.5 to 1:2.4 (w/w), electrical conductivity of the sequentially fabricated AgNW-LM-PDMS hybrid composite is superior to the AgNW-PDMS and LM-

PDMS composite. Moreover, it increases gradually with the LM content changing from  $8.43 \times 10^5$  to  $1.00 \times 10^6$  S m<sup>-1</sup> for the weight ratio of 1:0.5-1:2.4 (w/w). Whereas hybrid composites fabricated using the mixed approach show a decrease in electrical conductivity with increasing LM content varying from  $1.18 \times 10^6$  to  $7.15 \times 10^5$  S m<sup>-1</sup> for the same weight ratios. The 1:4 AgNW:LMP (w/w) ratio for both sequential and mixed hybrid composite displayed the lowest electrical conductivity among all the weight ratios of the hybrid composite; however, it was higher than the single-filler LM-PDMS composite. Single-filler LM composites containing LM particles in an elastomeric matrix possess lower conductivity than bulk LM even with a higher volume fraction of LM.<sup>24</sup> In the sequential approach, it can be seen that the electrical conductivity of AgNW-LM films decreases with the LM content, while it increases for the surface embedded AgNW-LM-PDMS hybrid composite. This is because the electrical conductivity in the film is dominated by LM, whereas AgNWs are the major contributors for electrical conductivity in the hybrid composite (unstrained state). The sheet resistances of the surface embedded AgNW-LM-PDMS hybrid composite (Figure 3b) with the sequential and mixed approaches varied from 0.127 to 0.104  $\Omega$  sq<sup>-1</sup> and from 0.080 to 0.106  $\Omega$  sq<sup>-1</sup>, respectively, with the increasing LM content.

Electromechanical behavior of the hybrid composites fabricated using the two approaches with different AgNW:LMP weight ratios were studied. Figure 3c-f shows the electromechanical performance (i.e., resistance change vs strain) of the composites until PDMS failure. For the same weight ratio of AgNW:LMP, the electromechanical performance of the sequential hybrid composite is superior to the mixed hybrid composite and the AgNW-PDMS composite. Moreover, electromechanical performance of the sequential AgNW-LM-PDMS hybrid composite improves with the increasing LM content. At 1:2.4 AgNW:LMP weight ratio; it becomes similar to that of the LM-PDMS composite. Figure 3c shows that at 90% strain, resistance change of the 1:2.4 (w/w) sequential AgNW-LM-PDMS hybrid composite is only 2.04%. As expected, resistance change of the LM-PDMS composite with strain remains low due to the intrinsic deformable nature of LM. Figure 4a,b displays the titled cross-sectional SEM images of sequential and mixed AgNW-LM-PDMS hybrid composites, respectively, under no strain and strain conditions. Under no strain, the sequential hybrid composite shows uniformly distributed coalesced LMPs and AgNWs. When stretched, the LMPs deform in the stretching direction and bridge the stretched AgNW network, thus preserving the electrical conductance. 45 Cross-sectional SEM images of the sequential hybrid composites in Figure S5a,b further reveal that LMPs can bridge the cracks formed in the AgNW network during stretching. 26,46 For the mixed hybrid composite, LMPs are trapped and segregated by AgNW skeleton. The high surface roughness prevents the LMPs from forming a uniform coalesced film. This is because the volume of LM trapped within the LMPs is insufficient to connect with the neighboring LMPs which are at a different height within the film. 41 When stretched, the locally sintered and entangled LMPs between the AgNWs separate, resulting in higher resistance. Cross-sectional SEM images of the mixed hybrid composite in Figure S5c show that LMPs do not bridge the cracks formed in the composite during stretching. Table S2 compares the electrical conductivity and quality factor between our work and reported literature utilizing conductive fillers in

an elastomeric matrix. 1,24,39,46-49 The mixed AgNW-LM-PDMS hybrid composite with a AgNW:LMP weight ratio of 1:0.5 demonstrated highest conductivity in the reported literature; meanwhile, the sequential hybrid composite with ratio 1:2.4 demonstrated the highest quality factor.

To further understand the electromechanical behaviors of the mixed and sequential hybrid composites, the interaction of LMPs and AgNWs in the laser sintered AgNW-LM films was probed using SEM and energy dispersive X-ray spectroscopy (EDS). Figure 5a-d shows top-view SEM images of the laser sintered AgNW-LM films with the sequential approach for the weight ratios of 1:0.5, 1:1.5, 1:2.4, and 1:4, respectively. For the ratios 1:0.5 and 1:1.5 (w/w), the formation of Ag-In aggregates occurred, which appear as whitish to light gray, surrounded by dark gray Ga-rich regions composed of Ga and In. 25 For the 1:4 ratio, rod-like whiskers composed of Ag and In formed. For the 1:2.4 ratio, Ag-In whiskers were observed in addition to the Ag-In aggregates. EDS analysis in Figure 4e shows that the Ag-In aggregates (points marked as 1-3 in the SEM image) in the 1:2.4 (w/w) AgNW-LM film are composed of an average 27.2 wt % of Ag and 70.2 wt % of In, with the corresponding atomic % values of 25.3 at. % Ag and 61.5 at. % In. Whereas, Ag-In whiskers (points marked as 4-6 in the SEM image) in the film are composed of an average 27.0 wt % of Ag and 69.0 wt % of In, with the corresponding atomic % values of 22.0 at. % Ag and 52.9 at. % In, suggesting the formation of AgIn<sub>2</sub> intermetallic compound in both aggregates and whiskers. Several mechanisms are known to contribute to whisker growth, such as stress generation and relaxation, interdiffusion, and phase transformation. 50 In this work, Ag-In alloying to form intermetallic compound (IMC) is responsible for whisker growth. During the IMC formation, in-plane compressive stresses build up in the film due to the large volume expansion. 51,52 To relieve these in-plane compressive stresses, a diffusion of Ag and In atoms occurs across the AgNW-LM interface to the surface, leading to the formation of whiskers. Whiskers appear at higher AgNW:LMP weight ratio (i.e., 1:2.4 and 1:4) due to increased number of reaction sites and availability of more In to continue the diffusion process. Figure 6 shows Ag-In whiskers observed through cross-

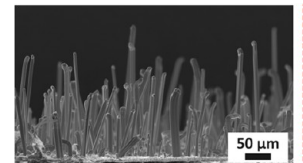




Figure 6. Cross-sectional view SEM image showing the formation of Ag-In whiskers in laser sintered sequentially fabricated AgNW-LM film with 1:4 AgNW:LMP (w/w). Inset showing zoomed image of Ag-In whiskers. Scale bar: 50  $\mu$ m.

sectional SEM image of 1:4 (w/w) AgNW-LM film. To further understand the Ag-In whiskers observed in this study, the selected area electron diffraction (SAED) pattern was studied through transmission electron microscopy (TEM). The whisker was lifted and thinned using a focused ion beam (FIB) as shown in Figure 7a. SAED confirmed the crystalline structure of the observed Ag-In whisker as AgIn2 along the [110] zone axis (Figure 7b). High-resolution EDS mapping of the whisker (Figure 7c) confirmed the presence of both Ag and In within the whiskers with a negligible amount of Ga. By contrast, the AgNW-LM film with the mixed approach did not

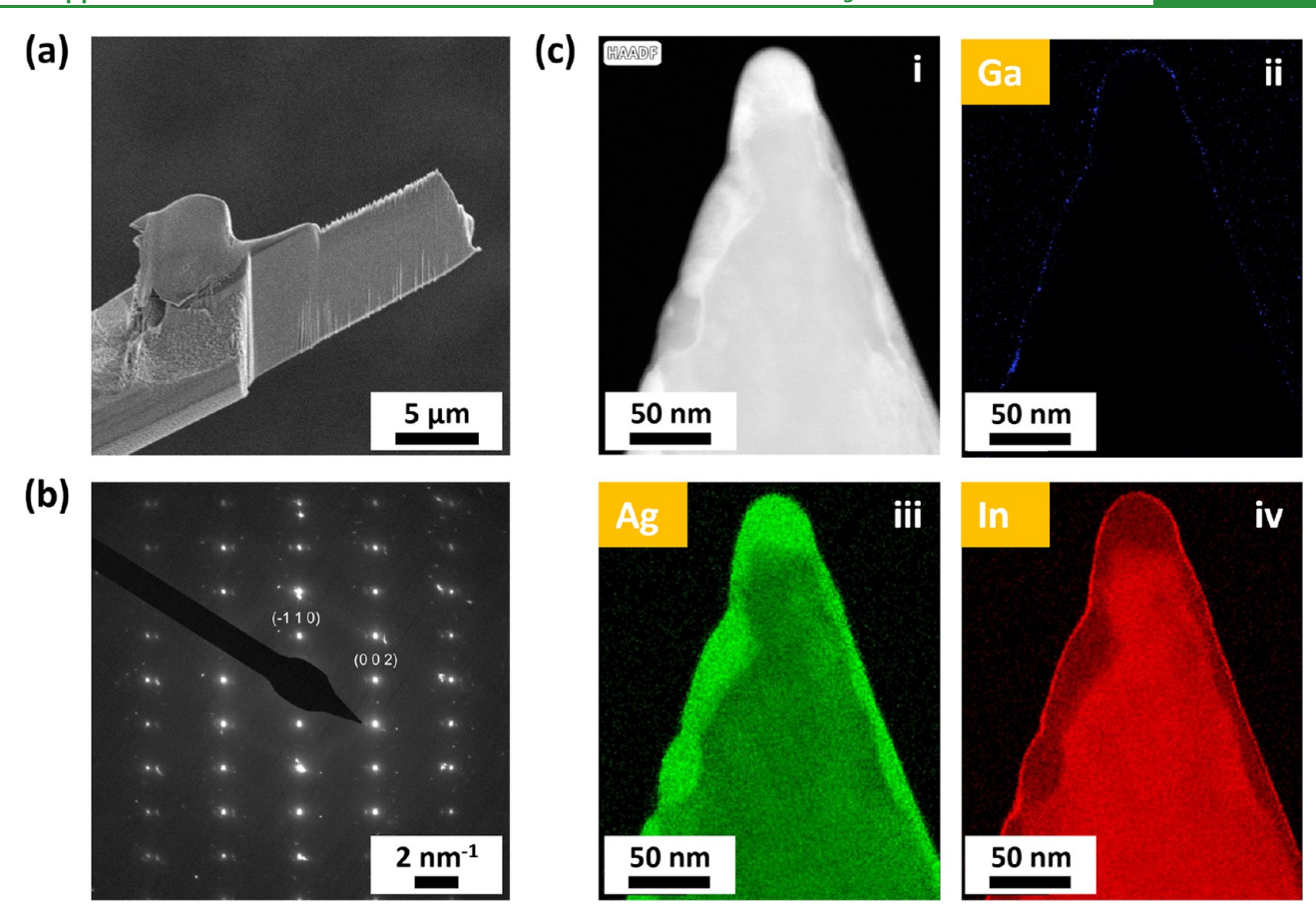


Figure 7. Transmission electron microscopy (TEM) characterization of the Ag-In whisker observed in laser sintered sequentially fabricated AgNW-LM film with 1:4 AgNW:LMP (w/w). (a) Focused ion beam (FIB) lifting and thinning of Ag–In whisker. Scale bar 5  $\mu$ m. (b) Selected area electron diffraction (SAED) pattern from the Ag-In whisker. Scale bar 5 nm<sup>-1</sup>. (c) Energy-dispersive X-ray spectroscopy (EDS) mapping of Ag-In whisker tip. Scale bar 50 nm.

show the formation of Ag-In aggregates or whiskers, as shown in the top-view SEM images in Figure S6a,b. In the mixed approach, LM particles were trapped and segregated by the AgNW skeleton, which prevents them from forming a connected network. In this arrangement, effective sintering of the LM particles becomes more difficult: Only lower laser power could be applied; higher laser power could cause burning of the surrounding AgNWs due to higher laser absorbance of AgNWs.44 Additionally, it has been reported that the  $AgIn_2$  alloy is typically formed protruding from the LM surface.<sup>23</sup> In the sequential approach, the top layer is composed of a bed of laser sintered LM. Figure 5 shows that the AgIn<sub>2</sub> alloy rises above the LM bed. This has also been reported for sequential deposition of metals such as gold and gallium, where AuGa2 intermetallic compound appears on the liquid Ga surface.<sup>51</sup> Since the mixed approach lacks the formation of a continuous LM film (i.e., only comprising segregated LM droplets), it does not have the desired sites for the formation of AgIn2 alloy. These findings agreed with the works involving mixing the AgNWs and LM particles, which also did not report the formation of AgIn2 intermetallic compound.33

EDS mapping in Figure 8 provides further insights into the bonding mechanism of the sequentially fabricated AgNW-LM films. For all the AgNW:LMP weight ratios, it can be seen that throughout the film where the Ga concentration is high, the Ag concentration is low, or vice versa. Additionally, In can be seen to be distributed throughout the AgNW-LM film, mostly

bonded with Ag and some bonded with Ga.<sup>53</sup> Hence, a biphasic (solid-liquid) Ag-In-Ga system forms consisting of Ga-In as LM droplets and AgIn<sub>2</sub> as intermetallic compounds. We reason that the high affinity between Ag and In can improve the adhesion between AgNWs and LMPs in the film by anchoring LMPs to AgNWs. The Ag-In bonding, in addition to the Ga-In bonding, provides mechanical robustness and the large deformability of the Ag-In-Ga system.

Mechanical robustness of the sequential hybrid composite was investigated. Two types of tests, scratching and peeling, were carried out on 1:2.4 (w/w) AgNW-LM-PDMS sequential hybrid composite, as well as with the AgNW-PDMS and LM-PDMS composites for comparison. First, scratching was performed on all three composites with the sharp edge of a razor blade. Figure 9a shows that the sequential hybrid composite and the LM-PDMS composite maintained stable resistance not only with increasing number of scratches but also with two deep cuts. The resistance change with eight scratches was 15%, which was very close to that of the LM-PDMS composite. The shearing force applied during scratching causes the LM to break from its oxide shell<sup>56</sup> and spread over the compromised region (Figure 9b), maintaining a stable electrical connection.<sup>27</sup> For the AgNW-PDMS composite, the resistance increased considerably, e.g.,  $\Delta R/R_0 = 1.49$  with eight scratches, due to the absence of a liquid-like conductive filler such as EGaIn. The AgNW-PDMS composite became nonconductive after one cut. Next, a peel

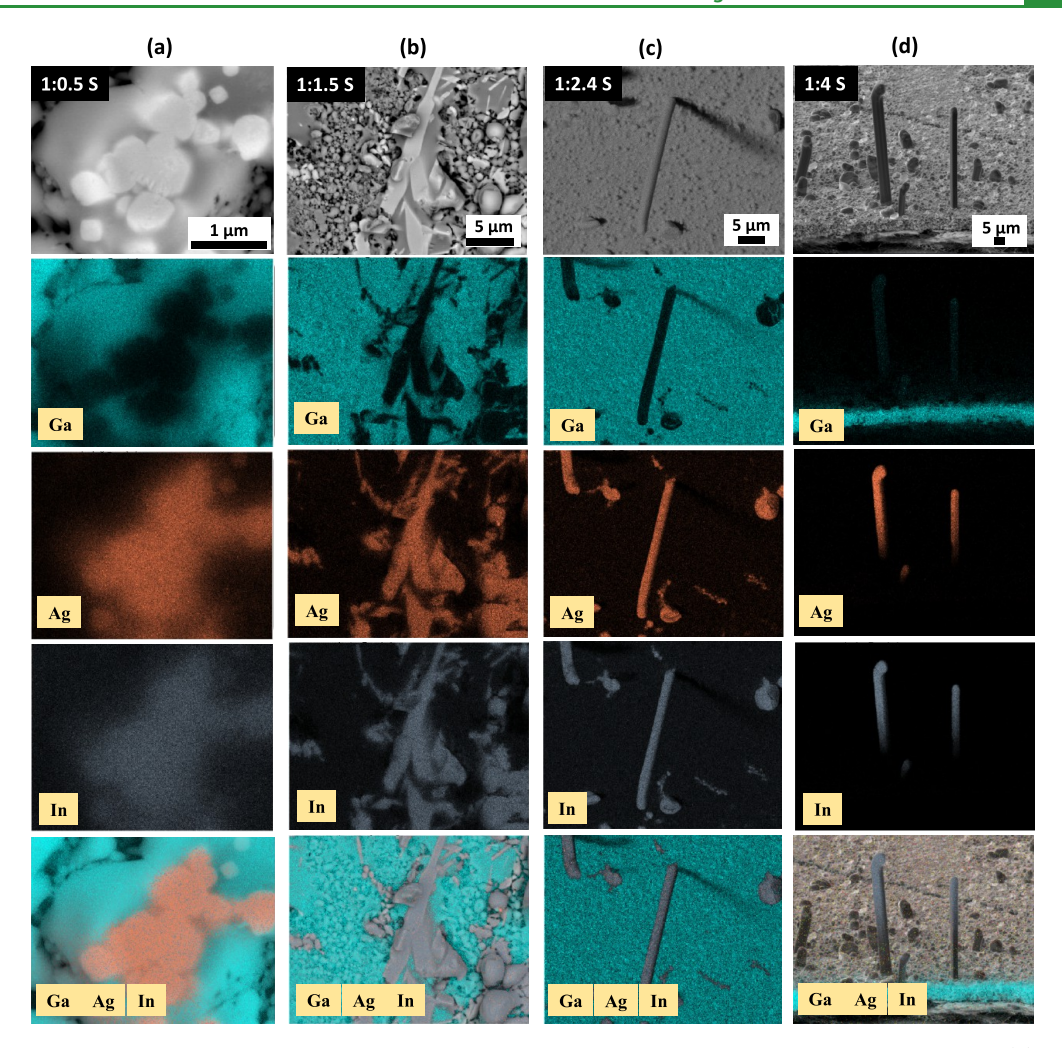


Figure 8. Top-view SEM images and EDS surface mapping analysis for AgNW-LM film fabricated using sequential approach (S) with AgNW:LMP weight ratios of (a) 1:0.5 (scale bar:  $1 \mu m$ ), (b) 1:1.5, (c) 1:2.4, and (d) 1:4 (Scale bar:  $5 \mu m$ ).

test was performed by applying 3M Scotch tape on the composite and peeling it off. LM is known for its smearing nature. This is also evident in the peel test as seen in Figure 9c, where the resistance of the LM-PDMS composite increases with the peeling number. The resistance increases dramatically, e.g.,  $\Delta R/R_0 = 196.5$  after 70 repeats of peeling. The optical image in Figure S7a shows the extent of LM transferred onto the 3M Scotch tape after peeling it from the LM-PDMS composite. On the contrary, the surface embedded AgNW-LM-PDMS hybrid composite mimics the behavior of the AgNW-PDMS composite and shows a resistance change of only 65% with 75 repeats of peeling. Note that a fresh piece of tape was used each time. Video S1 shows that the hybrid composite is also robust against wiping with no obvious removal of LM after repeated wiping with an ethanol soaked Kimtech wipe. This can be attributed to the surface embedded structure of the AgNW-LM-PDMS hybrid composite, which plays a key role in providing the desired mechanical robustness. Additionally, strong Ag-In bonds observed through the AgIn<sub>2</sub> alloy formation in the Ag-In-Ga system contributes to the nonsmearing behavior of the hybrid composite.<sup>59</sup> Figure S7b,c shows the performance of the mixed AgNW-LM-PDMS hybrid composite in the scratch/cut and peel test, respectively. The performance of the hybrid

composites from the mixed approach was inferior to the ones from the sequential approach.

To evaluate cyclic stability under strain, the sequential AgNW-LM-PDMS hybrid composite was tested under 60% tensile cyclic strain, as shown in Figure 9d. The resistance changed to a maximum of 2.1% after 900 cycles of loading and unloading, showcasing the cyclic stability of the hybrid composite. Table S3 compares the performance of the AgNW-PDMS, LM-PDMS, and sequentially fabricated AgNW-LM-PDMS hybrid composite. The hybrid composite displayed electromechanical stability similar to the LM-PDMS composite and superior to the AgNW-PDMS composite. In terms of patternability, the hybrid composite can be laser patterned into different designs, as shown in Figures 10 and 11, without the need of a mold or an encapsulation layer.

To demonstrate the application potential of the AgNW-LM-elastomer sequential hybrid composite, a laser patterned textile-based stretchable heater and a stretchable LED circuit were fabricated. Thermal therapy can not only reduce pain caused by sports related injuries but also treat diseases such as osteoarthritis. Heat improves blood flow in the tissue which reduces stiffness and inflammation providing better muscle extensibility. In this work, after laser sintering the AgNW-LM film, thermoplastic polyurethane (TPU) was spin coated on top. The film was cured to form a surface embedded

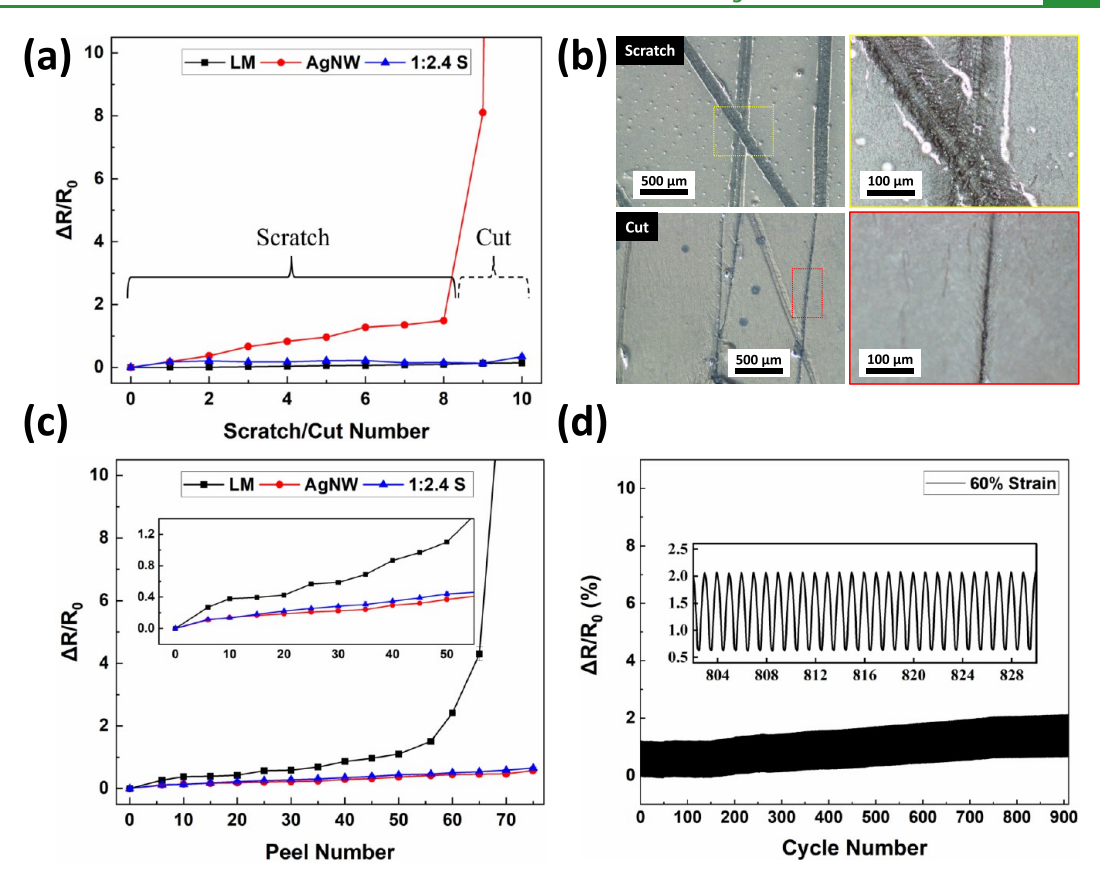


Figure 9. (a) Resistance change as a function of scratch and cut number for AgNW-PDMS, LM-PDMS, and surface embedded AgNW-LM-PDMS hybrid composite from sequential (S) approach (AgNW:LMP = 1:2.4 wt %). (b) Optical images of scratched and cut regions on sequentially fabricated 1:2.4 (AgNW:LMP w/w) surface embedded AgNW-LM-PDMS hybrid composite. Scale bar: 500  $\mu$ m. Insets showing zoomed areas for scratch and cut, respectively. Scale bar: 100  $\mu$ m. (c) Resistance change as a function of peel number for AgNW-PDMS, LM-PDMS, and surface embedded AgNW-LM-PDMS hybrid composite (AgNW:LMP = 1:2.4 wt %) from sequential (S) approach. (d) Resistance changes after 900 tensile stretching and releasing cycles at 60% strain for sequentially fabricated 1:2.4 (W) surface embedded AgNW-LM-PDMS hybrid composite. Inset showing resistance change between cycle number 803 to 829.

AgNW-LM-TPU hybrid composite. The hybrid composite was then laser cut to the desired shape and heat pressed onto the textile.<sup>64</sup> Stepwise voltage ranging from 0 to 5.5 V was applied to the textile-based heater as depicted in Figure 10a. The temperature of the heater increased with the applied voltage and at 5.5 V the maximum temperature recorded was ~110 °C. Commercial heating pads usually operate at multiple heat settings with the highest temperature of ~70 °C. The temperature range of the textile-based heater at 4.5 V was between 58 and 77 °C, and hence further testing was performed at 4.5 V. Figure 10b shows the infrared (IR) thermal image of the heater under 0 and 4.5 V. The stability of the heater under repeated heating and cooling cycles was studied due to its crucial role in wearable application. Each cycle in Figure 10c was characterized by 30 s of heating at 4.5 V and 30 s of natural cooling. The heater showed stable performance after 200 heating and cooling cycles with the temperature ranging between 34 and 47 °C. The heater could not recover back to the room temperature within 30 s due to the relatively low thermal transport properties of the textile. 65,66 For wearable application, the heater should be conformable and stretchable. Therefore, performance of the heater, when wrapped around a glass vial with 27.35 mm in diameter was studied (Figure S8a). A stretchability test was also performed to investigate the heating performance under tensile strain. Figure S8b shows that the textile-based heater

showed a resistance change of 6.55% at 65% strain. Figure 10d,e shows the temperature of the heater and the IR images, respectively, at different strains. The temperature of the heater dropped from 60 to 43 °C when the strain increased from 0 to 65%. Table S4 shows the current values at a constant voltage of 4.5 V for each strain level in Figure 10e. Figure 10f illustrates stable performance of the textile heater on a knee at various bending angles of 64°, 97°, 134°, and 180°.

For the other demonstration, a stretchable LED circuit was fabricated by laser patterning the surface embedded AgNW-LM-PDMS composite. LED lights were connected to the hybrid composite using silver paste. Next, a soft PDMS layer was spin coated on top to encapsulate the entire LED circuit. Figure 11 shows the stretchable LED circuit. The stretchable circuit shows stable performance until 57% tensile strain, with no obvious difference in the light intensity of the LEDs.

## 3. CONCLUSION

In this work, hybrid conductive composite films comprising AgNWs and EGaIn particles were fabricated using two different approaches—sequential and mixed—where the fillers were embedded below the surface of an elastomeric matrix. We investigated how AgNW and LM interact in the two fabrication processes, leading to very different structural morphologies and in turn material properties. Morphological characterization of the AgNW-LM film revealed that AgIn<sub>2</sub>

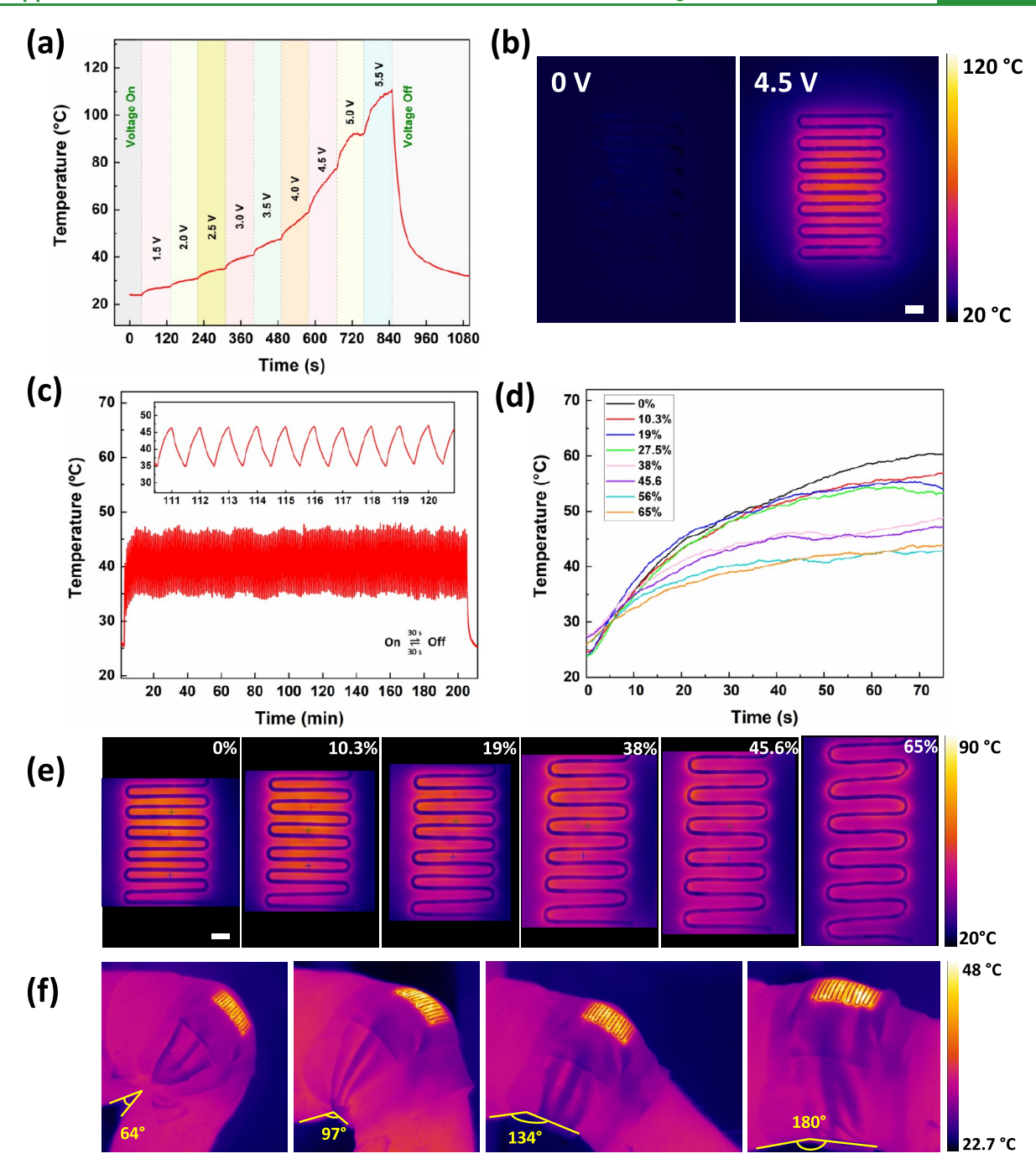


**Figure 10.** Surface embedded AgNW-LM-TPU based heater on textile. (a) Temperature evolution of heater under stepwise voltage from 0 to 5.5 V. (b) Infrared (IR) thermal image of the heater at 0 and 4.5 V. Scale bar: 5 mm. (c) Temperature evolution of the heater under repeated heating cycle operations (200 cycles). Inset showing heater performance between time period of 111–120 min. (d) Temperature as a function of tensile strain for the heater. (e) IR images of the heater at different strains. Scale bar: 5 mm. (f) IR images of the heater on the knee during different knee bending angles of 64°, 97°, 134°, and 180°.

intermetallic compounds were formed only using the sequential approach, pointing out the crucial role of different fabrication techniques. Formation of AgIn<sub>2</sub> intermetallic compounds along with Ga—In bonds was the key to imparting mechanical robustness and large deformability to the sequential hybrid composite. Moreover, different weight ratios of AgNW:LMP in the two approaches provided tunable electrical conductivity. In terms of electromechanical stability, the AgNW-LM-elastomer hybrid composites from both approaches performed better than the AgNW-elastomer composite. In particular, 1:2.4 (w/w) sequential AgNW-LM-

elastomer hybrid composite demonstrated the best electromechanical stability with a resistance increase of only 2.04% at 90% strain which was similar to the performance of LM-PDMS composite. The sequentially fabricated hybrid composite also possessed mechanical robustness against peeling, wiping, and scratching, which is a common issue with single filler conductive composites composed of LM or AgNWs. The AgNW-LM-elastomer based hybrid composite facilitated direct laser patterning, which is difficult with LM-based composites. To demonstrate the application for stretchable electronics, a

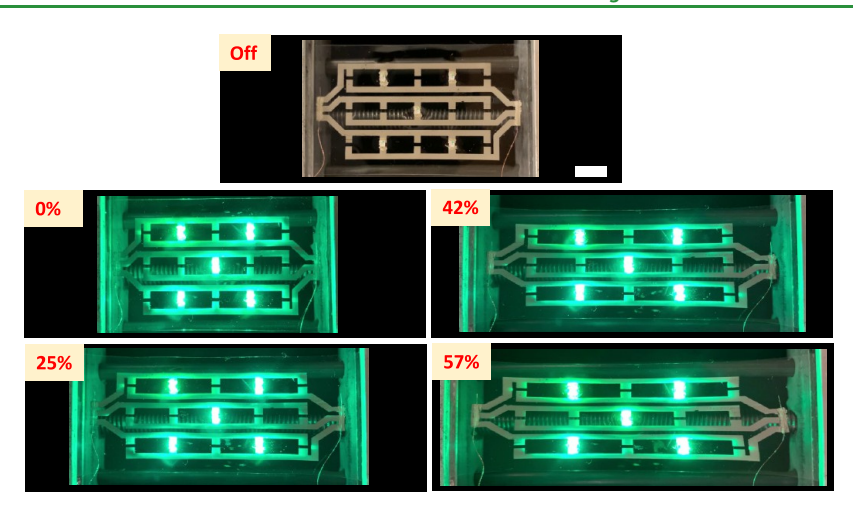


Figure 11. Surface embedded AgNW-LM-PDMS hybrid composite based stretchable LED circuit during off state and at different tensile strains of 25, 42%, and 57%. Scale bar: 8 mm.

laser patterned stretchable heater on textile and a stretchable LED circuit are fabricated.

#### 4. EXPERIMENTAL SECTION

**4.1. Preparation of AgNWs.** AgNWs were fabricated by a modified polyol process. First, 60 mL of 0.147 M polyvinylpyrrolidone (PVP) ( $M_{\rm v}\sim40\,000$ ; Sigma-Aldrich) solution in ethylene glycol (EG) was added to a three-necked round-bottomed flask that was suspended in an oil bath at 151.5 °C and was magnetically stirred at 260 rpm for 1 h. 200  $\mu$ L of 24 mM CuCl<sub>2</sub> (CuCl<sub>2</sub>·2H<sub>2</sub>O, 99.999+%; Alfa Aesar) solution in EG was added into the heated solution. After 15 min, 60 mL of 0.094 M AgNO<sub>3</sub> (99+%; Sigma-Aldrich) solution in EG was added to the flask. Upon nanowire formation, the solution was cooled to room temperature. Products were washed with acetone first, and then with ethanol. AgNWs were suspended in IPA for fabrication of AgNW-LM composite.

**4.2. Preparation of LM Particles (LMPs).** Liquid metal solution was prepared by adding 100  $\mu$ L of EGaIn in a glass vial with 10 mL of IPA. To make the LM particles solution, the mixture was probe sonicated for 20 min at an amplitude of 40%. During the sonication, the glass vial was suspended in an ice bath to prevent the IPA from evaporating. Prior to drop-casting, the solution was mixed vigorously to ensure a uniform dispersion of LMPs in IPA.

**4.3. Fabrication of AgNW-LM-Elastomer Composite.** *4.3.1. Sequential Approach.* A AgNW suspension in IPA containing 0.025 g of AgNWs was first drop-casted onto a precleaned glass slide and dried at 50 °C. Thermal annealing with an annealing temperature and time of 150 °C and 30 min, respectively was performed to fuse the AgNW junctions. Next, LMPs in IPA were drop-cast on top of the AgNWs and dried at room temperature to make AgNW-LMP films with different weight ratios of AgNW:LMP (same weight of AgNWs). The AgNW-LMP film was laser sintered using a VLS 6.60/75 laser writer. Laser settings (power and speed) were tuned depending upon the weight ratio of AgNW:LMP. To fabricate surface embedded AgNW-LM-PDMS hybrid composite, liquid PDMS (Sylgard 184, Dow Inc.) in the weight ratio of 10:1 of prepolymer to cross-linker was spin-coated on the AgNW-LM film and cured at 50 °C for 3h.

4.3.2. Mixed Approach. A AgNW suspension in IPA containing 0.025 g of AgNWs was mixed with different weight ratios of LMP. The mixed suspension was drop-casted on a precleaned glass slide and dried at 50 °C. The AgNW-LMP film was laser sintered at different laser settings depending upon the weight ratio of AgNW-LMP. To fabricate surface embedded AgNW-LM-PDMS hybrid composite, liquid PDMS was spin-coated on the AgNW-LM film and cured at 50 °C for 3h

**4.4. Characterization.** Sintering was performed using a 60 W  $CO_2$  based laser with a wavelength of 10.6  $\mu$ m (model VLS 6.60/75 from Universal Laser Systems). Morphologies of the AgNW-LM film

from sequential and mixed approach was studied using field emission scanning electron microscopy (FESEM) (FEI Quanta 3D FEG) operated at 5 kV. For cross-sectional SEM imaging, AgNW-LM films were fabricated on an silicon wafer. The silicon wafer was cleaved in liquid nitrogen environment to prevent leakage of LM. The SEM micrographs were collected in both secondary electrons (SE) and circular backscatter detector (CBS) modes. Energy dispersive spectroscopy (EDS) spot analysis and EDS surface mapping was done using the Helios 5 Hydra CX dual-beam SEM equipped with the advanced EDAX octane electron energy dispersive X-ray detector. Keyence VKX1100 confocal laser scanning microscope was used to measure the surface roughness and thickness of the AgNW-LM films. The Ag-In whisker was studied using transmission electron microscopy (TEM). For TEM, the sample was prepared using a ThermoFisher Quanta 3D FEG for Focused Ion Beam (FIB) lift-out and analyzed with a ThermoFisher Talos F200X TEM operating at 200 kV. EDS surface mapping on the Ag-In whisker was performed alongside TEM using the ThermoFisher Scientific SuperX EDS system with four Silicon Drift Detectors (SDD). A 4-probe method was used to measure the resistance of the printed lines using a digital multimeter (34401A, Keysight Technologies). The sheet resistance  $(R_s)$  was calculated using the formula  $R_s = (Rw)/L$  where R, w, and L are the resistance, width, and length of the AgNW-LM film traces. The electrical conductivity  $(\sigma)$  of the AgNW-LM films was calculated using  $\sigma = L/(RA)$  where L, R, and A are the length, resistance, and cross-sectional area of the AgNW-LM film traces. The length of the AgNW-LM film traces was 10 mm in both sheet resistance and electrical conductivity calculation. Stretchability analysis of all the composites was performed using a custom-made motorized linear stage and a digital multimeter (Keysight DAQ970A). Scratch and cut tests were performed by using a sharp-edged razor blade, while peel tests were performed using a 3M Scotch tape.

4.5. Fabrication of Textile-Based Heater and Stretchable LED Circuit. AgNW-LM film in the ratio of 1:2.4 w/w was fabricated using the sequential approach. After laser sintering, thermoplastic polyurethane (TPU) was spin coated and cured to form surface embedded AgNW-LM-TPU hybrid composite. Next, hybrid composite was patterned using the VLS 6.60/75 laser writer. The patterned heater was heat pressed on the textile (80% nylon and 20% Spandex with a thickness of 0.4 mm) using a heat press operated at a temperature of 150 °C for 3 min. Copper wires were connected using silver paste. For testing, a direct current (DC) power supply and an IR camera (FLIR A655sc) were used.

For stretchable LED circuit, AgNW-LM film was laser patterned into the desired shape and PDMS was spin coated to form surface embedded AgNW-LM-PDMS hybrid composite. LEDs were connected on the patterned circuit using silver paste. Stiff PDMS with 16.7% of curing agent was poured over the rigid LED locations

followed by spin coating the entire area with soft PDMS (6.3% curing agent) and curing at 50  $^{\circ}$ C for 3 h. The stretchable LED circuit was mounted on a manual tensile testing stage and powered using a DC power supply.

#### ASSOCIATED CONTENT

## **5** Supporting Information

The Supporting Information is available free of charge at https://pubs.acs.org/doi/10.1021/acsami.4c00318.

Schematic illustration of the preparation of liquid metal particles (LMPs), laser sintering conditions for the AgNW-LM films from sequential and mixed approach, optical images showing the glass substrates after peeling off surface embedded hybrid composite, morphologies of AgNW-LM films using confocal microscopy imaging, centrifuge tubes showing debris of entangled AgNWs and LMPs for mixed solutions, SEM images illustrating the behavior of the surface embedded hybrid composites under no strain and strain, comparison of electrical conductivity and quality factors between various literature reports using conductive filler, top-view SEM images of laser sintered AgNW-LM film from mixed approach, characterization of mechanical robustness of the mixed hybrid composite, comparison of different properties and behavior between AgNW-PDMS, LM-PDMS, and sequential AgNW-LM-PDMS hybrid composite, performance of surface embedded AgNW-LM-TPU based heater on textile, and variation of current with strain for the surface embedded AgNW-LM-TPU based heater on textile (PDF)

Video S1: Mechanical robustness of sequentially fabricated hybrid composite against repeated wiping with an ethanol soaked Kimtech wipe (MP4)

#### AUTHOR INFORMATION

## **Corresponding Author**

Yong Zhu — Department of Mechanical and Aerospace Engineering, North Carolina State University, Raleigh, North Carolina 27695, United States; ⊙ orcid.org/0000-0002-3862-5757; Email: yzhu7@ncsu.edu

### Authors

Darpan Shukla – Department of Mechanical and Aerospace Engineering, North Carolina State University, Raleigh, North Carolina 27695, United States; ⊚ orcid.org/0000-0001-8404-6054

Hongyu Wang – Department of Mechanical and Aerospace Engineering, North Carolina State University, Raleigh, North Carolina 27695, United States

Omar Awartani – Department of Chemical and Biomolecular Engineering, North Carolina State University, Raleigh, North Carolina 27695, United States

Michael D. Dickey – Department of Chemical and Biomolecular Engineering, North Carolina State University, Raleigh, North Carolina 27695, United States; orcid.org/ 0000-0003-1251-1871

Complete contact information is available at: https://pubs.acs.org/10.1021/acsami.4c00318

## **Author Contributions**

D.S. designed and conducted all the experiments. O.A. provided the liquid metal (eGaIn). H.W. and D.S. performed the SEM and EDS analysis. Y.Z. supervised the research. O.A.

and M.D.D. contributed to the discussion. D.S., M.D.D., and Y.Z. wrote the manuscript with input from all the authors. All authors gave approval to the final version of the manuscript.

#### Notes

The authors declare no competing financial interest.

## ACKNOWLEDGMENTS

The authors would like to acknowledge the financial support from the National Science Foundation under award no. 2134664.

#### REFERENCES

- (1) Lopes, P. A.; Fernandes, D. F.; Silva, A. F.; Marques, D. G.; de Almeida, A. T.; Majidi, C.; Tavakoli, M. Bi-Phasic Ag-In-Ga-Embedded Elastomer Inks for Digitally Printed, Ultra-Stretchable, Multi-Layer Electronics. ACS Appl. Mater. Interfaces 2021, 13 (12), 14552–14561.
- (2) Dickey, M. D. Stretchable and Soft Electronics Using Liquid Metals. *Adv. Mater.* **2017**, 29 (27), 1606425.
- (3) Kim, D.-H.; Lu, N.; Ma, R.; Kim, Y.-S.; Kim, R.-H.; Wang, S.; Wu, J.; Won, S. M.; Tao, H.; Islam, A.; Yu, K. J.; Kim, T.; Chowdhury, R.; Ying, M.; Xu, L.; Li, M.; Chung, H.-J.; Keum, H.; McCormick, M.; Liu, P.; Zhang, Y.-W.; Omenetto, F. G.; Huang, Y.; Coleman, T.; Rogers, J. A. *Epidermal Electronics. Science* (1979) **2011**, 333 (6044), 838–843.
- (4) Lipomi, D. J.; Vosgueritchian, M.; Tee, B. C.-K.; Hellstrom, S. L.; Lee, J. A.; Fox, C. H.; Bao, Z. Skin-like Pressure and Strain Sensors Based on Transparent Elastic Films of Carbon Nanotubes. *Nat. Nanotechnol* **2011**, *6* (12), 788–792.
- (5) Kaltenbrunner, M.; Sekitani, T.; Reeder, J.; Yokota, T.; Kuribara, K.; Tokuhara, T.; Drack, M.; Schwödiauer, R.; Graz, I.; Bauer-Gogonea, S.; Bauer, S.; Someya, T. An Ultra-Lightweight Design for Imperceptible Plastic Electronics. *Nature* **2013**, 499 (7459), 458–463.
- (6) Yao, S.; Swetha, P.; Zhu, Y. Nanomaterial-Enabled Wearable Sensors for Healthcare. *Adv. Healthc Mater.* **2018**, 7 (1), 1700889.
- (7) Yao, S.; Zhu, Y. Nanomaterial-Enabled Stretchable Conductors: Strategies, Materials and Devices. *Adv. Mater.* **2015**, *27* (9), 1480–1511
- (8) Hu, L.; Yuan, W.; Brochu, P.; Gruner, G.; Pei, Q. Highly Stretchable, Conductive, and Transparent Nanotube Thin Films. *Appl. Phys. Lett.* **2009**, 94 (16), 161108.
- (9) Gong, S.; Schwalb, W.; Wang, Y.; Chen, Y.; Tang, Y.; Si, J.; Shirinzadeh, B.; Cheng, W. A Wearable and Highly Sensitive Pressure Sensor with Ultrathin Gold Nanowires. *Nat. Commun.* **2014**, *5* (1), 3132.
- (10) Jang, H.; Park, Y. J.; Chen, X.; Das, T.; Kim, M.; Ahn, J. Graphene-Based Flexible and Stretchable Electronics. *Adv. Mater.* **2016**, 28 (22), 4184–4202.
- (11) Xu, F.; Zhu, Y. Highly Conductive and Stretchable Silver Nanowire Conductors. *Adv. Mater.* **2012**, *24* (37), 5117–5122.
- (12) Wang, X.; Li, J.; Song, H.; Huang, H.; Gou, J. Highly Stretchable and Wearable Strain Sensor Based on Printable Carbon Nanotube Layers/Polydimethylsiloxane Composites with Adjustable Sensitivity. ACS Appl. Mater. Interfaces 2018, 10 (8), 7371–7380.
- (13) Kwon, C.; Seong, D.; Ha, J.; Chun, D.; Bae, J.; Yoon, K.; Lee, M.; Woo, J.; Won, C.; Lee, S.; Mei, Y.; Jang, K.; Son, D.; Lee, T. Self-Bondable and Stretchable Conductive Composite Fibers with Spatially Controlled Percolated Ag Nanoparticle Networks: Novel Integration Strategy for Wearable Electronics. *Adv. Funct Mater.* **2020**, 30 (49), 2005447.
- (14) Tehrani, F.; Beltrán-Gastélum, M.; Sheth, K.; Karajic, A.; Yin, L.; Kumar, R.; Soto, F.; Kim, J.; Wang, J.; Barton, S.; Mueller, M.; Wang, J. Laser-Induced Graphene Composites for Printed, Stretchable, and Wearable Electronics. *Adv. Mater. Technol.* **2019**, 4 (8), 1900162.
- (15) Song, J.; Kim, Y.; Kang, K.; Lee, S.; Shin, M.; Son, D. Stretchable and Self-Healable Graphene-Polymer Conductive Com-

- posite for Wearable EMG Sensor. Polymers (Basel) 2022, 14 (18), 3766.
- (16) Wang, J.; Cai, G.; Li, S.; Gao, D.; Xiong, J.; Lee, P. S. Printable Superelastic Conductors with Extreme Stretchability and Robust Cycling Endurance Enabled by Liquid-Metal Particles. *Adv. Mater.* **2018**, *30* (16), 1706157.
- (17) Yoshida, A.; Wang, Y.-F.; Sekine, T.; Takeda, Y.; Kumaki, D.; Tokito, S. Printed Low-Hysteresis Stretchable Strain Sensor Based on a Self-Segregating Conductive Composite. *ACS Applied Engineering Materials* **2023**, *1* (1), 50–58.
- (18) Yang, Y.; Duan, S.; Zhao, H. Advances in Constructing Silver Nanowire-Based Conductive Pathways for Flexible and Stretchable Electronics. *Nanoscale* **2022**, *14* (32), 11484–11511.
- (19) Liang, J.; Tong, K.; Pei, Q. A Water-Based Silver-Nanowire Screen-Print Ink for the Fabrication of Stretchable Conductors and Wearable Thin-Film Transistors. *Adv. Mater.* **2016**, 28 (28), 5986—5996.
- (20) Sivan Pillai, A.; Chandran, A.; Kuzhichalil Peethambharan, S. Silver Nanoparticle-Decorated Multiwalled Carbon Nanotube Ink for Advanced Wearable Devices. ACS Appl. Mater. Interfaces 2022, 14 (41), 46775–46788.
- (21) Yun, G.; Tang, S.-Y.; Lu, H.; Zhang, S.; Dickey, M. D.; Li, W. Hybrid-Filler Stretchable Conductive Composites: From Fabrication to Application. *Small Science* **2021**, *1* (6), 2000080.
- (22) Zheng, Y.; Li, Y.; Dai, K.; Wang, Y.; Zheng, G.; Liu, C.; Shen, C. A Highly Stretchable and Stable Strain Sensor Based on Hybrid Carbon Nanofillers/Polydimethylsiloxane Conductive Composites for Large Human Motions Monitoring. *Compos. Sci. Technol.* **2018**, *156*, 276–286.
- (23) Tavakoli, M.; Malakooti, M. H.; Paisana, H.; Ohm, Y.; Green Marques, D.; Alhais Lopes, P.; Piedade, A. P.; de Almeida, A. T.; Majidi, C. EGaIn-Assisted Room-Temperature Sintering of Silver Nanoparticles for Stretchable, Inkjet-Printed, Thin-Film Electronics. *Adv. Mater.* 2018, 30 (29), 1801852.
- (24) Saborio, M. G.; Cai, S.; Tang, J.; Ghasemian, M. B.; Mayyas, M.; Han, J.; Christoe, M. J.; Peng, S.; Koshy, P.; Esrafilzadeh, D.; Jalili, R.; Wang, C. H.; Kalantar-Zadeh, K. Liquid Metal Droplet and Graphene Co-Fillers for Electrically Conductive Flexible Composites. *Small* **2020**, *16* (12), 1903753.
- (25) Silva, A. F.; Paisana, H.; Fernandes, T.; Góis, J.; Serra, A.; Coelho, J. F. J.; de Almeida, A. T.; Majidi, C.; Tavakoli, M. High Resolution Soft and Stretchable Circuits with PVA/Liquid-Metal Mediated Printing. *Adv. Mater. Technol.* **2020**, 5 (9), 2000343.
- (26) Pan, X.; Guo, D.; He, H. Novel Conductive Polymer Composites Based on CNTs/CNFs Bridged Liquid Metal. *J. Phys. D Appl. Phys.* **2021**, *54* (8), 085401.
- (27) Lin, Y.; Genzer, J.; Dickey, M. D. Attributes, Fabrication, and Applications of Gallium-Based Liquid Metal Particles. *Advanced Science* **2020**, *7* (12), 2000192.
- (28) Wu, S.; Yao, S.; Liu, Y.; Hu, X.; Huang, H. H.; Zhu, Y. Buckle-Delamination-Enabled Stretchable Silver Nanowire Conductors. *ACS Appl. Mater. Interfaces* **2020**, *12* (37), 41696–41703.
- (29) Huang, Q.; Zhu, Y. Patterning of Metal Nanowire Networks: Methods and Applications. ACS Appl. Mater. Interfaces 2021, 13 (51), 60736–60762.
- (30) Zhou, W.; Yao, S.; Wang, H.; Du, Q.; Ma, Y.; Zhu, Y. Gas-Permeable, Ultrathin, Stretchable Epidermal Electronics with Porous Electrodes. *ACS Nano* **2020**, *14* (5), 5798–5805.
- (31) Lee, P.; Lee, J.; Lee, H.; Yeo, J.; Hong, S.; Nam, K. H.; Lee, D.; Lee, S. S.; Ko, S. H. Highly Stretchable and Highly Conductive Metal Electrode by Very Long Metal Nanowire Percolation Network. *Adv. Mater.* **2012**, 24 (25), 3326–3332.
- (32) Liang, J.; Tong, K.; Pei, Q. A Water-Based Silver-Nanowire Screen-Print Ink for the Fabrication of Stretchable Conductors and Wearable Thin-Film Transistors. *Adv. Mater.* **2016**, *28* (28), 5986–5996.
- (33) Cho, C.; Shin, W.; Kim, M.; Bang, J.; Won, P.; Hong, S.; Ko, S. H. Monolithically Programmed Stretchable Conductor by Laser-

- Induced Entanglement of Liquid Metal and Metallic Nanowire Backbone. Small 2022, 18 (37), 2202841.
- (34) Kim, M.; Park, J. J.; Cho, C.; Ko, S. H. Liquid Metal Based Stretchable Room Temperature Soldering Sticker Patch for Stretchable Electronics Integration. *Adv. Funct Mater.* **2023**, 33 (36), 2303286.
- (35) Kim, M.; Cho, C.; Shin, W.; Park, J. J.; Kim, J.; Won, P.; Majidi, C.; Ko, S. H. Nanowire-Assisted Freestanding Liquid Metal Thin-Film Patterns for Highly Stretchable Electrodes on 3D Surfaces. *npj Flexible Electronics* **2022**, *6* (1), 99.
- (36) Lin, Y.; Fang, T.; Bai, C.; Sun, Y.; Yang, C.; Hu, G.; Guo, H.; Qiu, W.; Huang, W.; Wang, L.; Tao, Z.; Lu, Y.; Kong, D. Ultrastretchable Electrically Self-Healing Conductors Based on Silver Nanowire/Liquid Metal Microcapsule Nanocomposites. *ACS Nano Lett.* 2023, 23 (23), 11174–11183.
- (37) Korte, K. E.; Skrabalak, S. E.; Xia, Y. Rapid Synthesis of Silver Nanowires through a CuCl- or CuCl 2 -Mediated Polyol Process. *J. Mater. Chem.* **2008**, *18* (4), 437–441.
- (38) Liu, Y.; Wang, H.; Zhu, Y. Recycling of Nanowire Percolation Network for Sustainable Soft Electronics. *Adv. Electron Mater.* **2021**, 7 (9), 2100588.
- (39) Sun, Y.; Han, X.; Guo, P.; Chai, Z.; Yue, J.; Su, Y.; Tan, S.; Sun, X.; Jiang, L.; Heng, L. Slippery Graphene-Bridging Liquid Metal Layered Heterostructure Nanocomposite for Stable High-Performance Electromagnetic Interference Shielding. *ACS Nano* **2023**, *17* (13), 12616–12628.
- (40) Kim, S.; Kim, S.; Hong, K.; Dickey, M. D.; Park, S. Liquid-Metal-Coated Magnetic Particles toward Writable, Nonwettable, Stretchable Circuit Boards, and Directly Assembled Liquid Metal-Elastomer Conductors. ACS Appl. Mater. Interfaces 2022, 14 (32), 37110–37119.
- (41) Liu, S.; Yuen, M. C.; White, E. L.; Boley, J. W.; Deng, B.; Cheng, G. J.; Kramer-Bottiglio, R. Laser Sintering of Liquid Metal Nanoparticles for Scalable Manufacturing of Soft and Flexible Electronics. ACS Appl. Mater. Interfaces 2018, 10 (33), 28232–28241.
- (42) Lin, Y.; Cooper, C.; Wang, M.; Adams, J. J.; Genzer, J.; Dickey, M. D. Handwritten, Soft Circuit Boards and Antennas Using Liquid Metal Nanoparticles. *Small* **2015**, *11* (48), 6397–6403.
- (43) Liu, S.; Reed, S. N.; Higgins, M. J.; Titus, M. S.; Kramer-Bottiglio, R. Oxide Rupture-Induced Conductivity in Liquid Metal Nanoparticles by Laser and Thermal Sintering. *Nanoscale* **2019**, *11* (38), 17615–17629.
- (44) Frey, E. J.; Im, S.; Bachmann, A. L.; Genzer, J.; Dickey, M. D. Patterning of a High Surface Area Liquid Metal-Carbon Composite Film Using Laser Processing. *Adv. Funct Mater.* **2023**, 2308574.
- (45) Zolfaghari, N.; Khandagale, P.; Ford, M. J.; Dayal, K.; Majidi, C. Network Topologies Dictate Electromechanical Coupling in Liquid Metal-Elastomer Composites. *Soft Matter* **2020**, *16* (38), 8818–8825.
- (46) Liu, Z.; Chen, S.; Zhang, G.; Shi, H.; Chen, X.; Shi, W.; Liu, L. Interfacial Engineering for Highly Stable and Stretchable Electrodes Enabled by Printing/Writing Surface-Embedded Silver and Its Selective Alloying with Liquid Metals. *Adv. Mater. Interfaces* **2022**, 9 (11), 2102121.
- (47) Silva, C. A.; lv, J.; Yin, L.; Jeerapan, I.; Innocenzi, G.; Soto, F.; Ha, Y.; Wang, J. Liquid Metal Based Island-Bridge Architectures for All Printed Stretchable Electrochemical Devices. *Adv. Funct Mater.* **2020**, *30* (30), 2002041.
- (48) Li, Y.; Feng, S.; Cao, S.; Zhang, J.; Kong, D. Printable Liquid Metal Microparticle Ink for Ultrastretchable Electronics. *ACS Appl. Mater. Interfaces* **2020**, *12* (45), 50852–50859.
- (49) Zu, W.; Ohm, Y.; Carneiro, M. R.; Vinciguerra, M.; Tavakoli, M.; Majidi, C. A Comparative Study of Silver Microflakes in Digitally Printable Liquid Metal Embedded Elastomer Inks for Stretchable Electronics. *Adv. Mater. Technol.* **2022**, *7* (12), 2200534.
- (50) Zhang, P.; Zhang, Y.; Sun, Z. Spontaneous Growth of Metal Whiskers on Surfaces of Solids: A Review. J. Mater. Sci. Technol. 2015, 31 (7), 675–698.

www.acsami.org

- (51) Hirsch, A.; Michaud, H. O.; Gerratt, A. P.; de Mulatier, S.; Lacour, S. P. Intrinsically Stretchable Biphasic (Solid-Liquid) Thin Metal Films. *Adv. Mater.* **2016**, 28 (22), 4507–4512.
- (52) Majumdar, B. S.; Dutta, I.; Bhassyvasantha, S.; Das Mahapatra, S. Recent Advances in Mitigation of Whiskers from Electroplated Tin. *JOM* **2020**, *72* (2), 906–917.
- (53) Wang, P. J.; Kim, J. S.; Lee, C. C. Intermetallic Reaction of Indium and Silver in an Electroplating Process. *J. Electron. Mater.* **2009**, 38 (9), 1860–1865.
- (54) Yu, C.-F.; Cheng, H.-C.; Chen, W.-H. Structural, Mechanical, Thermodynamic and Electronic Properties of AgIn 2 and Ag 3 In Intermetallic Compounds: Ab Initio Investigation. *RSC Adv.* **2015**, *5* (86), 70609–70618.
- (55) Zhang, J.; Lu, Q.; Li, Y.; Li, T.; Lu, M.-H.; Chen, Y.-F.; Kong, D. An Ultrastretchable Reflective Electrode Based on a Liquid Metal Film for Deformable Optoelectronics. *ACS Mater. Lett.* **2021**, 3 (8), 1104–1111.
- (56) Lin, Y.; Genzer, J.; Li, W.; Qiao, R.; Dickey, M. D.; Tang, S.-Y. Sonication-Enabled Rapid Production of Stable Liquid Metal Nanoparticles Grafted with Poly(1-Octadecene- Alt -Maleic Anhydride) in Aqueous Solutions. *Nanoscale* **2018**, *10* (42), 19871–19878.
- (57) Yang, J.; Nithyanandam, P.; Kanetkar, S.; Kwon, K. Y.; Ma, J.; Im, S.; Oh, J. H.; Shamsi, M.; Wilkins, M.; Daniele, M.; Kim, T. il; Nguyen, H. N.; Truong, V. K.; Dickey, M. D. Liquid Metal Coated Textiles with Autonomous Electrical Healing and Antibacterial Properties. *Adv. Mater. Technol.* **2023**, 8 (14), 2202183.
- (58) Markvicka, E. J.; Bartlett, M. D.; Huang, X.; Majidi, C. An Autonomously Electrically Self-Healing Liquid Metal-Elastomer Composite for Robust Soft-Matter Robotics and Electronics. *Nat. Mater.* **2018**, *17* (7), 618–624.
- (59) Hajalilou, A.; Silva, A. F.; Lopes, P. A.; Parvini, E.; Majidi, C.; Tavakoli, M. Biphasic Liquid Metal Composites for Sinter-Free Printed Stretchable Electronics. *Adv. Mater. Interfaces* **2022**, 9 (5), 2101913.
- (60) Valdes, K.; Marik, T. A Systematic Review of Conservative Interventions for Osteoarthritis of the Hand. *Journal of Hand Therapy* **2010**, 23 (4), 334–351.
- (61) Cui, Z.; Poblete, F. R.; Zhu, Y. Tailoring the Temperature Coefficient of Resistance of Silver Nanowire Nanocomposites and Their Application as Stretchable Temperature Sensors. *ACS Appl. Mater. Interfaces* **2019**, *11* (19), 17836–17842.
- (62) Wu, S.; Cui, Z.; Baker, G. L.; Mahendran, S.; Xie, Z.; Zhu, Y. A Biaxially Stretchable and Self-Sensing Textile Heater Using Silver Nanowire Composite. *ACS Appl. Mater. Interfaces* **2021**, *13* (49), 59085–59091.
- (63) Michlovitz, S.; Hun, L.; Erasala, G. N.; Hengehold, D. A.; Weingand, K. W. Continuous Low-Level Heat Wrap Therapy Is Effective for Treating Wrist Pain11A Commercial Party with a Direct Financial Interest in the Results of the Research Supporting This Article Has Conferred or Will Confer a Financial Benefit on the Author or/or More of the Authors. *Arch Phys. Med. Rehabil* **2004**, 85 (9), 1409–1416.
- (64) Yao, S.; Yang, J.; Poblete, F. R.; Hu, X.; Zhu, Y. Multifunctional Electronic Textiles Using Silver Nanowire Composites. *ACS Appl. Mater. Interfaces* **2019**, *11* (34), 31028–31037.
- (65) Shukla, D.; Liu, Y.; Zhu, Y. Eco-Friendly Screen Printing of Silver Nanowires for Flexible and Stretchable Electronics. *Nanoscale* **2023**, *15* (6), 2767–2778.
- (66) Wang, Y.; Yu, Z.; Mao, G.; Liu, Y.; Liu, G.; Shang, J.; Qu, S.; Chen, Q.; Li, R. Printable Liquid-Metal@PDMS Stretchable Heater with High Stretchability and Dynamic Stability for Wearable Thermotherapy. *Adv. Mater. Technol.* **2019**, *4* (2), 1800435.
- (67) Yuan, W.; Wu, X.; Gu, W.; Lin, J.; Cui, Z. Printed Stretchable Circuit on Soft Elastic Substrate for Wearable Application. *Journal of Semiconductors* **2018**, 39 (1), 015002.